The Global Precipitation Measurement (GPM) Mission for Science and Society

Gail Skofronick-Jackson[1], Walter A. Petersen[2], Wesley Berg[3], Chris Kidd[4], Erich F. Stocker[1], Dalia B. Kirschbaum[1], Ramesh Kakar[5], Scott A. Braun[1], George J. Huffman[1], Toshio Iguchi[6], Pierre E. Kirstetter[7], Christian Kummerow[3], Robert Meneghini[1], Riko Oki[8], William S. Olson[9], Yukari N. Takayabu[10], Kinji Furukawa[8], Thomas Wilheit[11]

Corresponding Author: Gail Skofronick-Jackson, Gail.S.Jackson@nasa.gov, 301-614-5720
NASA Goddard Space Flight Center, Code 612, Building 33, Room A405, 8800 Greenbelt Rd, Greenbelt, MD 20771 USA

[1]NASA Goddard Space Flight Center, 8800 Greenbelt Rd, Greenbelt, MD 20771 USA
[2]NASA Marshall Space Flight Center, NSSTC, 320 Sparkman Drive, Huntsville, AL, 35805 USA
[3]Colorado State University, Fort Collins, CO 80523-1371 USA
[4]University of Maryland, College Park, Greenbelt, MD 20740, USA
[5]NASA Headquarters, Washington, DC USA
[6]National Institute of Information and Communications Technology (NICT), Tokyo, Japan
[7]NOAA/National Severe Storms Laboratory, 120 David L. Boren Blvd, Norman OK 73072-7303, USA
[8]Japan Aerospace Exploration Agency, Tokyo, Japan
[9]Joint Center for Earth Systems Technology, University of Maryland Baltimore County, Baltimore, MD USA
[10]The University of Tokyo, Tokyo, Japan
[11]Texas A&M University, College Station, TX, USA

Submitted 1 August 2016

Revised 18 April 2019

Capsule: The Global Precipitation Measurement (GPM) mission collects essential rain and snow data for scientific studies and societal benefit.

Abstract—Precipitation is a key source of freshwater; therefore observing global patterns of precipitation and its intensity is important for science, society, and understanding our planet in a changing climate. In 2014, NASA and the Japan Aerospace Exploration Agency (JAXA) launched the Global Precipitation Measurement (GPM) Core Observatory (GPM-CO) spacecraft. The GPM-CO carries the most advanced precipitation sensors currently in space including a dual-frequency precipitation radar provided by JAXA measuring the three-dimensional structures of precipitation and a well-calibrated, multi-frequency passive microwave radiometer providing wide-swath precipitation data. The GPM-CO was designed to measure rain rates from 0.2-110.0 mm h^{-1} and to detect moderate to intense snow events. The GPM-CO serves as a reference for unifying the data from a constellation of partner satellites to provide next-generation, merged precipitation estimates globally and with high spatial and temporal resolutions. Through improved measurements of rain and snow, precipitation data from GPM provides new information such as: details on precipitation structure and intensity; observations of hurricanes and typhoons as they transition from the tropics to mid-latitudes; data to advance near-real-time hazard assessment for floods, landslides and droughts; inputs to improve weather and climate models; and insights into agricultural productivity, famine, and public health. Since launch, GPM teams have calibrated satellite instruments, refined precipitation retrieval algorithms, expanded science investigations, and processed and disseminated precipitation data for a range of applications. The current status of GPM, its ongoing science, and future plans will be presented.

Introduction and Motivation

Water is essential to our planet, Earth. It literally moves mountains through erosion; transports heat in Earth's oceans and atmosphere; keeps our planet from freezing due to radiative impacts of atmospheric water vapor; causes catastrophes through droughts, floods, landslides, blizzards, and severe storms; but most importantly water is vital for nourishing all life on Earth. Precipitation as a source of freshwater links the Earth's water and energy cycles. Thus knowing when, where, and how precipitation falls is of paramount importance for science and society.

While there are areas of the world that have dense ground-based sensors for measuring precipitation in the form of rain gauges and radars, the vast oceans, less populated regions, and parts of developing countries lack adequate surface measurements of precipitation (Kidd et al. 2016). Satellites provide an optimal platform from which to measure precipitation globally. In 1997, NASA and the National Space Development Agency of Japan (NASDA), now the Japan Aerospace Exploration Agency (JAXA), launched the Tropical Rainfall Measuring Mission (TRMM) (Simpson et al. 1998, Kummerow et al. 1998, 2000), which operated until April 2015. The TRMM spacecraft had both a passive microwave multi-frequency imaging radiometer (provided by NASA) and a Ku-band radar channel (provided by NASDA) capable of generating three-dimensional views of precipitation structure (Kozu et al. 2001). TRMM's data continue to foster important scientific investigations such as Curtis et al. (2007), Adler et al. (2009), Shepherd et al. (2011), Liu et al. (2012), Houze et al. (2015), and Liu and Zipser (2015). In addition, TRMM has a large user community that has applied these data operationally to support decision making (Kirschbaum et al., 2016).

The Global Precipitation Measurement (GPM) Core Observatory (GPM-CO) spacecraft is an advanced successor to TRMM, with additional channels on both the Dual-frequency Precipitation Radar (DPR) and on the GPM Microwave Imager (GMI) with capabilities to sense light rain and falling snow (Hou et al. 2014, Hou et al. 2008). The GPM-CO, also a NASA-JAXA partnership, was launched in February 2014 and currently operates in a non-sun-synchronous orbit with an inclination angle of 65^{o}. This orbit allows the GPM-CO to sample precipitation across all hours of the day from the tropics to the Arctic and Antarctic circles and for observing hurricanes and typhoons as they transition from the tropics to mid-latitudes. GPM expands TRMM's reach not only in terms of global coverage, but also through sophisticated satellite instrumentation, the inter-calibration of datasets from other microwave radiometers, coordinated merged precipitation data sets, reduced latency for delivering data products, simplified data access, expanded global ground validation efforts, and integrated user applications. Because of the application focus of GPM, the public release of precipitation products is required in near-real-time (1-5 hours after the observations are downlinked to the ground stations).

The GPM mission has several scientific objectives including (1) advancing precipitation measurements from space, (2) improving knowledge of precipitation systems, water cycle variability and freshwater availability, (3) improving climate modeling and prediction, (4) improving weather forecasting and four-dimensional (4D) reanalysis, and (5) improving hydrological modeling and prediction. More details about these scientific objectives can be found in Hou et al. (2014).

The GPM-CO well-calibrated instruments allow for scientifically-advanced observations of precipitation in the mid-latitudes where a majority of the Earth's population lives. The central

panel of Figure 1 shows the coverage of the GPM-CO, and several interesting precipitation events are shown in panels a-l. These examples indicate the breadth of GPM's observational capabilities through measurements of diverse weather systems, such as severe convection, falling snow, light rain, and frontal systems over both land and ocean. The measurements include surface precipitation rates available from GMI and 3-dimensional precipitation structure from DPR.

A founding concept of the GPM mission is the constellation of precipitation observations provided by national and international satellite partners of opportunity. International and national partnerships are formed independently by both NASA and JAXA for sharing satellite data, ground validation measurements, and scientific expertise (Hou et al. 2014). The GPM-CO serves as a calibrator to ensure unified precipitation estimates from all satellite partners at high temporal (0.5 to 3.0 hours) and spatial (5 to 15 km) scales (Hou et al. 2014). Such satellite precipitation datasets can be merged via algorithms and accumulated over time as shown in Figure 2. These GPM products allow for detailed investigations of how and where precipitation is distributed and how these patterns change over days, seasons, and years. These estimates are also used to model and estimate hazard impacts (e.g. floods and droughts), weather related disasters, agricultural forecasting, and famine warnings (Kirschbaum et al., 2016).

The GPM-CO instruments and constellation concept will be discussed in Section 2. Precipitation retrieval algorithms, data products, processing, and availability will be presented in Section 3. Section 4 will be devoted to early validation results. In Section 5, the paper will summarize how GPM data have been used over the past two years for selected scientific investigations and societal applications. Material presented herein is primarily from the U.S. Science Team. Nevertheless, it is important to note that the current and future successes of GPM

are joint with our international partners, especially Japan. The paper will close with conclusions and next steps.

GPM Core Observatory and Constellation Configuration

An essential activity of the GPM mission is the use of the NASA-JAXA GPM-CO to unify and inter-calibrate data sets generated by constellation satellite partners and merge these into next-generation, high temporal resolution global precipitation estimates. Fundamental to the success of this activity is both the GPM-CO instrumentation and the constellation configuration.

GPM Core Observatory

The GPM-CO was launched February 28, 2014 at 3:37am JST (February 27, 2014 18:37 UTC) from Tanegashima Island, Japan. The prime mission lifetime (instrument design life) is 3 years and 2 months (for checkout) but fuel is projected to last well beyond that, potentially lasting 15 or more years if the instruments/spacecraft systems (e.g., batteries) do not fail and fuel requirements do not increase. The GMI and DPR together provide a powerful synergistic tool to assess precipitation micro- and macro-structure, intensity and phase globally at relatively high (regional) resolutions. The DPR with Ku-band (35.5 GHz) and Ka-band (13.6 GHz) channels provides three-dimensional (3D) precipitation (rain and snow) particle structure with vertical resolution of 250m, a horizontal resolution of ~5 km, and swath width of 125 km (Ka) and 245 km (Ku) (Hou et al. 2014). The DPR was extensively calibrated pre-launch (Kojima et al., 2013) and its performance meets mission requirements (e.g., Kubota et al. 2015, Kubota et al. 2016, Toyoshima et al. 2015). (See also the sidebar on GPM's Mission Science Requirements.)

The GMI is a 13 channel conically scanning microwave radiometer (see Table 1 and Hou et al. 2014 for details). GMI provides wide-swath (885 km) TB data to estimate surface precipitation at resolutions ranging from 5-25 km depending on frequency. Design requirements for GMI were driven both by requirements to build *a priori* databases to support Bayesian microwave precipitation retrieval algorithms (Kummerow et al. 2010, Kummerow et al. 2015) as well as to provide a reference radiance calibration standard for the GPM constellation (Hou et al. 2014). The design features needed to meet the requirements include a shroud over the warm load to eliminate solar intrusions, a robust reflective antenna coating to minimize emissivity issues, and the addition of noise diodes for a four point calibration of the window channels (Draper et al. 2013, 2015a, 2015b). The GMI instrument is meeting its performance requirements (Draper et al. 2015) and has already been deemed one of the best calibrated conically scanning passive microwave radiometers in space with brightness temperature accuracy for all channels within 0.4K and stability within 0.2K (Wentz and Draper, 2016).

GPM Constellation Configuration

The GPM mission encompasses the GPM-CO and a constellation of about 10 satellites (as of mid-2016) from national and international partners of opportunity [see Table 1 and Hou et al. 2014 for details]. These satellites are designed and operated for the partners' missions, but these agencies are willing to share their data with GPM for the purpose of producing next-generation unified global precipitation estimates. The constellation satellites bearing passive radiometers fly independent polar or non-sun-synchronous orbits allowing for multiple coincident overpasses with the GPM-CO.

For the constellation partner data, the first step toward unified precipitation estimates is the inter-calibration of brightness temperatures (TB) using GMI as the reference standard. This ensures that the observed TB are consistent among the sensors with expected differences after accounting for variations in the observing frequencies, bandwidths, polarizations, and view angles (see Wilheit 2013, Wilheit et al. 2015, Zavodsky et al. 2013, Zhang et al. 2011, 2016 and Table 1). Figure 3 shows the extent of coverage provided by single 98-minute orbits for each of the various radiometer types in the GPM constellation.

Sensor inter-calibration between GMI and the partner sensors involves several steps, as described in Wilheit (2013, 2015) and Berg et al. (2016). Multiple independent approaches are compared during these steps, which help to identify flaws or limitations of a given approach, thus increasing confidence in the results and providing a measure of the uncertainty in the resulting calibration adjustments. After adjustments, residual differences between GMI channels and those on the constellation radiometers are generally smaller than 1 K (Berg et al. 2016). This is a remarkable achievement that now allows the project to focus on the precipitation products rather than TB uncertainties.

Future satellite inter-calibration tasks include understanding and quantifying the residual uncertainties in the estimated calibration differences due to the radiative transfer models and geophysical parameter retrievals and adapting to changes in the radiometer constellation. Updates in the GMI calibration algorithms and subsequent inter-calibration adjustments to the constellation sensors will occur during scheduled reprocessing of retrieval products. In addition, inter-calibrating TRMM's TMI and pre-GPM microwave constellation sensor data to GMI is necessary

for generating a consistent long-term next-generation precipitation record that covers the TRMM and GPM eras.

Algorithms, Data Products, Data Processing and Data Availability

The GPM-CO data processing is a joint NASA/JAXA effort. NASA data processing is done at GSFC (Greenbelt, MD) in the Precipitation Processing System (PPS). JAXA data processing is carried out at the Tsukuba Space Center (Tsukuba, Ibaraki, Japan) in the Mission Operations System (MOS). The interconnected architecture of this joint mission ground system can be seen in Figure 4. Working with the GPM principal investigators and science algorithm developers, PPS maintains the operational science data processing system and ensures the timely processing of all GPM science instrument data [see Hou et al. 2014 for a table of GPM products]. During routine operations, raw instrument data (Level 0 data) is received in near-real-time by the PPS and processed using science algorithms to produce calibrated, swath-level instrument (Level 1, L1) data. JAXA's MOC processes DPR Level 1 products and their Level 3 merged satellite products. Additional algorithms are used to compute geophysical parameters such as precipitation rate at the swath-level resolution (Level 2, L2 data products). [For reference, a special collection of papers describing the L2 precipitation algorithms is appearing in the *Journal of Atmospheric and Oceanic Technology*.] At the final stage of processing, Level 3 (L3) algorithms produce gridded and accumulated geophysical parameters including products such as latent heating profiles (e.g., Tao et al. 2016). It is envisioned that Level 4 data products developed through model-assimilated precipitation forecast and analysis will be available in the future.

208 The GPM mission has both near-real-time (NRT) and research-quality production
209 requirements. Both NASA and JAXA contribute key processing efforts to fulfill these latency
210 requirements. The NRT products are produced using forecast or earlier forms of ancillary data.
211 NRT products include GMI TB, and precipitation estimates from GMI (denoted GPROF),
212 DPR, and Combined Radar-Radiometer Algorithm (denoted CORRA) (Kummerow et al. 2015,
213 Seto et al. 2015, Grecu et al. 2016). GMI products are available within an hour of data collection
214 while DPR and CORRA are available within 3 hours of data collection. Another NRT product
215 developed by the U.S. team is the Integrated Multi-satellitE Retrievals for GPM (IMERG) gridded
216 retrieval that is a Level 3 NASA product (Huffman et al. 2015). JAXA produces an analogous
217 product called Global Satellite Mapping of Precipitation (GSMaP) (Kubota et al. 2007, Aonashi
218 et al. 2009, Ushio et al. 2009). IMERG uses the GPM-CO to inter-calibrate precipitation data from
219 all constellation radiometers. Temporal and spatial gaps in the IMERG microwave precipitation
220 estimates (e.g., as shown in Figure 3) are filled by morphing the estimates in between the microwave
221 overpasses, and incorporating IR estimates with a Kalman filter where the gaps are too long (over
222 about 3 hours) to produce 0.1º x 0.1º half-hour global products. The IMERG product is produced
223 twice in NRT; once approximately 5 hours after data collection and again approximately 14 hours
224 after data collection.
225 All of the NRT products are also processed as research products. The geolocation of the
226 research products is more consistent as predictive ephemeris rarely needs to be used. Research
227 products are produced by PPS when all the required high quality ancillary and geolocation data
228 are received with the objective for accuracy, completeness, and consistency. These research
229 products are available hours to months after data collection and are stable for long-term

precipitation investigations. PPS generates and distributes all data from the instruments on the core satellite as well as Level 2 and Level 3 data from the partner constellation satellites. In addition to the standard HDF5 format files, a Geographic Information System (GIS; TIFF world files) product and ASCII text files are provided for selected product estimates. All GPM data are openly available and accessible from https://pmm.nasa.gov/data-access/downloads/gpm. JAXA's GPM products in general can be obtained from https://www.gportal.jaxa.jp/gp/top.html while the GSMaP multi-satellite merged data can be obtained from http://sharaku.eorc.jaxa.jp/. GPM data (Level 0-3) are periodically reprocessed as retrieval algorithms are improved. The at-launch Version 03 IMERG accumulation products are known to be high biased during heavy rain events and the next IMERG reprocessing to Version 04 (early 2017) is expected to address these high biases. GPM retrieval algorithms use the dual frequency channels of DPR and the high frequency channels of GMI and hence precipitation products from GPM are different than those from TRMM. Nevertheless, there are plans to reprocess inter-calibrated precipitation data (in winter 2017-2018) to produce a consistent long-term precipitation record that starts at the beginning of TRMM. GPM is meeting data latency requirements (as shown in the sidebar), on average, greater than 99% of the time. Recent PPS statistics show nearly 50 TB data downloaded by more than 1,000 unique users from all over the world in a single month.

Validation Efforts

GPM Ground Validation (GV) efforts include the direct statistical validation and verification of satellite estimates against high-quality ground measurements, and physical validation for algorithm improvement and hydrological models. Validating data is from both regular ongoing surface observations and focused field campaigns (Hou et al., 2014; see also

https://pmm.nasa.gov/index.php?q=science/ground-validation). Major GPM validation efforts are: (1) Comparisons among satellite precipitation products, (2) comparisons against ground datasets, and (3) analysis for meeting mission requirements.

One evaluation technique compares zonal means among the various GPM instrument algorithms and established precipitation estimates such as the Global Precipitation Climatology Project (GPCP) data sets (Adler et al. 2003) and, over ocean, the Merged CloudSat, TRMM, Aqua version 2 (MCTA2) data (Behrangi et al. 2014). Both GPCP and MCTA2 include a variety of input data sets selected for utility in precipitation estimation at both low and high latitudes. Figure 5 shows the global zonal means for 2015 for land and ocean (Figure 5a), ocean only (Figure 5b), and land only (Figure 5c). This figure illustrates that DPR, Ku, CORRA, and GPROF algorithm retrievals are in good agreement. The GPM zonal accumulations underestimate with respect to the MCTA at higher latitudes. This is most attributable to the fact that the DPR minimum detectable reflectivities correspond to minimum rain rates of approximately 0.2 mm h^{-1}. Since much of the higher latitude precipitation is light, and CORRA and GPROF are based on DPR estimates, GPM is low in the higher latitudes. A high latitude, light precipitation solution for GPROF is being implemented in the upcoming algorithm Version 05 release. The mean daily precipitation in mm day^{-1} for each of the algorithms is provided in Table 2. This table shows that IMERG annual precipitation is lower than the other algorithms while there are interesting differences among the diverse approaches over land. Land surfaces tend to complicate the retrieval process and the various algorithms use different approaches to mitigate surface (emissivity and clutter) issues.

Direct statistical GV of GPM rainfall rate estimates relies primarily on existing high-resolution, quality-controlled U.S. national radar network rain rate products such as the NOAA

National Severe Storms Laboratory/University of Oklahoma Multi-Radar/Multi-Sensor (MRMS) products (e.g., Zhang et al., 2016 and references therein). Currently, the MRMS system (http://mrms.ou.edu) incorporates data from all polarimetric WSR-88D radars (NEXRAD), a large number of automated rain gauge networks, and model analyses in the Continental U.S. (CONUS) and southern Canada. The system creates a gridded mosaic of quantitative precipitation estimates (QPE) products on a 0.01° x 0.01° grid at a 2-minute temporal resolution (Zhang et al. 2016 for most recent updates). Of particular value to GPM GV are MRMS radar-based gauge-adjusted QPE. Collectively, these MRMS products provide an independent and consistent reference for directly evaluating post-launch GPM precipitation products across a large number of meteorological regimes as a function of resolution, accuracy, and sample size (Kirstetter et al. 2012).

For continental scale verification of GPM products over CONUS all MRMS data coincident with GPM orbits are continuously processed and saved as a GPM GV dataset (http://wallops-prf.gsfc.nasa.gov/NMQ/index.html). In addition to standard MRMS quality control procedures (see Zhang et al. 2016), additional procedures to minimize radar uncertainties are employed to derive a high-quality precipitation reference at the satellite product pixel resolution (Kirstetter et al. 2012). Filtering out instances when the radar-gauge ratios are outside of the range 0.1-10.0 further refines the instantaneous gauge bias-corrected MRMS product. In addition only radar data with the best measurement conditions (i.e., no beam blockage and radar beam below the melting layer) defined by a Radar Quality Index (RQI) are retained. Gridded 0.01° MRMS products can then be matched to allow direct comparisons between the surface radar and satellite precipitation products (see Figure 6).

296 Independent comparisons of this GPM GV-MRMS reference data set with two dense, well-
297 maintained, and data quality-controlled NASA rain gauge networks show that for c. 5 km footprint,
298 30 minute accumulations > 0.5 mm h^{-1}, biases are < 10% while normalized mean absolute errors
299 (NMAE) are < 35-40%. These results are consistent with a quantitative assessment of the MRMS
300 accuracy performed at its native resolution (Kirstetter et al. 2015b). Individual satellite radar
301 matches are subsequently averaged to coarser 50 km grids, useful for quick look comparison
302 products (cf. http://wallops-prf.gsfc.nasa.gov/NMQ/index.html) and for verifying GPM Level-1
303 science requirements (e.g., Figure 7). Here the increased spatial averaging of the footprints together
304 with removal of outliers (5^{th} and 95^{th} percentile) maintains low-bias while further reducing random
305 error in the MRMS data relative to the 5 km footprint scale mentioned above.
306 The GPM-GV MRMS reference dataset and its derivatives have revealed and quantified
307 several aspects of satellite-estimated rainfall retrieval errors and uncertainties including
308 comparisons of rainfall detectability and rainfall rate distributions (Kirstetter et al. 2014),
309 separation of systematic biases and random errors (Kirstetter et al. 2012), regional precipitation
310 biases (Chen et al. 2013), influence of precipitation sub-pixel variability and surface (Kirstetter et
311 al. 2015b; Carr et al. 2015), and comparison between satellite products (Kirstetter et al. 2013, 2014;
312 Tan et al., 2016a, b).
313 Figure 6 provides an example of comparisons to GPM Core satellite products for
314 instantaneous sampling times (e.g., coincident swath and MRMS sample time) as a density-scatter
315 plot for individual near surface DPR sensor footprint scales (effective resolution 5 km). Here it is
316 important to note that the scatter of the data exhibited in Figure 6 is expected based on the
317 instantaneous nature of the comparison at high spatial resolution (e.g., effective FOV), and the

318 related intrinsic random error associated with matching associated precipitation estimates in time
319 and space between MRMS and GPM L2 data swaths. Comparisons at this scale are best interpreted
320 as a tool for evaluating the broader systematic bias behavior between GPM products using the GV
321 as a third reference.

322 In Figure 6 good agreement between the GV MRMS reference and the near surface DPR-
323 Normal Scan (NS) algorithm Version 04 is evident with a bias (defined as the mean relative error;
324 MRE) and normalized mean absolute error (NMAE) of only -9.8% and 51.7%, respectively. The
325 Normal Scan mode of DPR consists of retrievals using the Ku-band 245 km wide swath data. The
326 agreement is particularly good for rainrates in the 1.0 – 10.0 mm h^{-1} range. Note that the minimum
327 detectable signal of the DPR (~0.2 mm h^{-1}, in terms of rainfall) and partial beam filling are
328 responsible for scatterplot differences at very low rain rates. Contingency statistics for DPR NS
329 rain detection reveal that for ground "reference" rain rates > 0.2 mm h^{-1} (the lower requirement
330 threshold specified for DPR rain detection based on radar sensitivity), yield a DPR Probability of
331 Detection (POD) of 64%, False Alarm Rate of 9%, and Heidke Skill Score (HSS) of 37%.

332 GPM Mission Science Requirements (see sidebar) stipulate thresholds for detection, bias,
333 and random error (Hou et al., 2013). For example, rain rate estimates should exhibit a bias and
334 random error of ≤ 50% (25%) at rain rates of 1 mm h^{-1} (10 mm h^{-1}) for areas of 50 km x 50 km.
335 Figure 7 is presented for the DPR Normal Scan (NS) product as a preliminary example of assessing
336 bias and random error. For non-zero raining pixels in Figure 7, the bias in each reference rain bin is
337 computed as the MRE in percent while for the random error the NMAE is computed with the
338 systematic error (bias) removed. Figure 7 suggests that the above GPM Mission Science
339 Requirements have been met for the DPR example shown and the method used. While these results

are encouraging, work is ongoing to further test and refine methodologies for determining product-consistent lower rain rate thresholds for comparing GPM GPROF, CORRA, DPR, and MRMS datasets and for defining error types and to meet the other GPM Mission Science Requirements.

Initial Scientific Investigations and Applications

With two years worth of calibrated and validated precipitation estimates, GPM's data are being used for scientific studies (e.g., Liu and Liu 2016, Wentz and Meissner 2016, Panegrossi et al. 2016, and Prakash et al. 2016). Most of the science results are from investigations by members of the NASA Precipitation Measurement Missions science team (in 2016 consisting of 60 Principal Investigators from NASA centers and U.S. universities funded by NASA Headquarters while the Japanese PMM Science Team consists of 41 Principal Investigators). NOAA has a team of 16 investigators involved with GPM and more than 20 international no-cost teams also play important roles in GPM science and validation efforts. Herein, two scientific investigations are reported: falling snow retrievals and monsoon studies.

Scientifically, retrievals of falling snow from space represent an important data set for understanding the Earth's atmospheric, hydrological, and energy cycles. While satellite-based remote sensing provides global coverage of falling snow events, the science is relatively new and retrievals are still undergoing development addressing challenges such as those listed in Skofronick-Jackson et al. (2015). GPM's mission goal of estimating falling snow is demonstrated in an example from March 17, 2014, just 18 days after launch (Figure 1c). More generally, the GMI observed the average snow rate, maximum snow rate, and fraction of precipitation that fell as snow over the winter of 2014-2015 (Figure 8). While these snow estimates are not fully validated they do support the requirement that GPM detect falling snow. The high rates over the south-central states

may not be representative of typical winter conditions, but may have resulted from the occurrence of several heavy snow events in mid-late February of 2015 when GMI had good overpasses. Of particular note for this period were the large snowfall rates along the west coast of Canada and southern coast of Alaska, where coastal topography may enhance local snowfall rates.

Looking elsewhere, the GPM mission can track the advance and retreat of India's annual monsoon and the tropical storms that impact India's populations. As shown in Figure 9, GPM observes the detailed structure of the copious monsoon precipitation as it marches from south to north across India over the seasons, with Tropical Cyclone Hudhud (Oct 2014) on the left and Storm Roamu (May 2016) on the far right of the timeline. Figure 9 shows the advance of the monsoon season from offshore in May to inland by July, and the retreat back to the Bay of Bengal from September to November over two years of GPM data. Over longer precipitation records, interannual variations due to the effect of large-scale oceanic or atmospheric patterns or to climate change may be identified, information that is crucial for societal applications and benefit.

Integrating satellite observations into land surface modeling systems is a critical component of how to resolve the state of the water cycle and stresses on the system during extreme events. The NASA Land Information System (LIS; Kumar et al. 2006, Peters-Lidard et al. 2007) runs operationally at the Short-term Prediction Research and Transition (SPoRT, 2016) Center (Jedlovec 2013, Zavodsky et al. 2013, Case et al. 2016) at NASA's Marshall Space Flight Center (Xia et al. 2012, Zhang et al. 2016, Vargas et al. 2015) to produce analyses and short term forecasts of soil moisture and other fields. LIS is a land surface modeling and data assimilation framework designed to integrate satellite observations, including GPM and the Soil Moisture Active Passive (SMAP) satellite data (Entekhabi et al., 2010) into the modeling infrastructure

(http://lis.gsfc.nasa.gov/). The integration of GPM data within LIS, run operationally at SPoRT, can capture soil moisture changes. For example, LIS identified an extreme soil moisture increase the first week of October 2015 when a closed upper low over the Southeastern U.S. combined with a deep tropical moisture plume associated with Hurricane Joaquin, led to historic rainfall over the Carolinas. The SPoRT Center provided model outputs from LIS to Eastern Region NWS forecast offices in near-real-time. In other cases, these data are also used by a variety of end users experimentally for assessing drought, flooding potential, and situational awareness for wildfire and blowing dust. There is great potential in the future for using GPM estimates together with other space-based soil-moisture measurements from SMAP to improve weather and hydrological prediction.

The GPM suite of products contributes to a wide range of societal applications such as: tropical cyclone location and intensity, famine early warning, drought monitoring, water resource management, agriculture, numerical weather prediction, land system modeling, global climate modeling, disease tracking, economic studies, and animal migration; many of which were initially developed with TRMM data. Many of these applications require near-real-time data as well as longer-term, well-calibrated precipitation information. IMERG is starting to be used as an input for forecasts in other regions of the world, especially areas lacking adequate ground-based coverage. Selected applications are reported in Kirschbaum et al. (2016), Ward et al. (2015), Kucera et al. (2013), and Kirschbaum and Patel (2016).

Conclusions and Next Steps

406 The Global Precipitation Measurement mission provides unprecedented and highly useful
407 global precipitation datasets. GPM's Core Observatory data are used to inter-calibrate a set of
408 precipitation observations from constellation partner sensors. By merging GPM multi-satellite
409 estimates with other IR satellite data, products with temporal resolutions down to 30 minutes and
410 spatial resolutions as small as 0.1^{o} by 0.1^{o} are possible. Latencies, at 1-5 hours (depending on the
411 product) after data collection, are vital for GPM's operational users. Research quality products
412 (with accuracy requirements as indicated in the Sidebar GPM's Mission Science Requirements)
413 are available later (12 hrs to several months) for intensive scientific studies ranging from
414 diagnosing microphysical precipitation particle characteristics to assessing regional and global
415 patterns of precipitation. The GPM mission provides indispensable precipitation data from micro
416 to local to global scales via retrieved precipitation particle size distributions inside clouds, 5-15
417 km resolution estimates of regional precipitation, and merged global precipitation.

418 GPM's algorithms have been updated several times (currently on Version 04) with an
419 additional update planned for 2017. After the release of Version 05, work will begin to reprocess
420 Level 0-3 products back to the beginning of TRMM (1998) and also for partner satellite data sets
421 to establish a long and consistent record of precipitation. Scientific studies and societal
422 applications using GPM data are ongoing and growing rapidly. Knowing the horizontal and
423 vertical structure of precipitation is important for improving weather forecasting and climate
424 change models. The planned processing of a consistent precipitation record encompassing the
425 TRMM and GPM era will be of high value to future generations of scientific studies and user
426 applications. The consistent TRMM-plus-GPM record will generate interesting scientific insights
427 and re-invigorate applications in hydrological/land surface modeling and numerical weather

prediction. Going forward in time, GPM's prime mission lifetime lasts until May 2017 at which time GPM will move into Extended Operations. Current predictions suggest that the station-keeping fuel will last 15 or more years, implying that instruments or spacecraft systems (like the batteries) will likely be the life-limiting factors as long as the fuel requirements do not increase.

In quantifying precipitation, a key Earth system component, the GPM mission provides fundamental knowledge of the water cycle and compliments other NASA satellite missions such as the Gravity Recovery and Climate Experiment (GRACE), that measures changes in groundwater levels in underground aquifers (among other observations) (Tapley et al. 2004); the Soil Moisture Active Passive (SMAP) satellite (Entekhabi et al. 2010); Aquarius (while it was operating), that observed ocean salinity (Le Vine et al. 2010); and CloudSat, which measures the properties of clouds and light precipitation (Stephens et al. 2002). Integrated multidisciplinary scientific investigations can provide greater understanding of our complex Earth system. GPM has and will continue to provide valuable and freely accessible precipitation data for science and society.

Acknowledgments

This paper is dedicated to former GPM Project Scientist Arthur Y. Hou (1947-2013). Data are provided by NASA / JAXA. The climatological monsoon dates are from the Indian Meteorology Department. Imagery was generated by NASA Goddard Space Flight Center, including the monsoon visualization by Owen Kelley. PMM Science Team members are acknowledged for their many contributions to GPM science. We thank our three anonymous reviewers for thoughtful and

paper-enhancing comments. Funding for this work was provided by NASA Headquarters, NOAA, and JAXA.

Sidebar 1: GPM's Mission Science Requirements

Prior to the GPM's launch in 2014, NASA formally documented Core Observatory requirements to be met within GPM's 3-year Prime Mission operations period in order for GPM to be deemed fully successful. Several of these requirements dealt with instrument performance or operational elements (e.g., orbit maintained to within ±1 km of operational orbital attitude) and will not be discussed here. Most of the requirements pertained to scientific accuracy and science data and are key to ensuring stable and validated precipitation products expected by both scientific investigators and application users. Specifically, these science requirements are:

- Measurements of the same geophysical scenes using both active and passive technique from 65°N to 65°S latitude with mean sampling time of 24 hours
- Using the DPR:
  - Quantify rain rates between 0.22 and 110.00 mm h^{-1}
  - Detect snowfall at an effective resolution of 5 km
- Using the GMI
  - Quantify rain rates between 0.2 and 60.0 mm h^{-1}
  - Detect snowfall at an effective resolution of 15 km
- Estimate precipitation particle size distribution (e.g., quantitative estimates of precipitation microphysical properties such as the mean median mass diameter of particle size distribution to within ±0.5 mm.)

- Provide calibrated ground-based precipitation measurements and associated error characterizations at 50 km horizontal resolution for comparison with space-based radar and radiometer measurements at designated ground validation sites within ground tracks of the GPM Core Observatory.
  - The biases in instantaneous rain rates between the ground-based and space-based estimates should not exceed 50% at 1 mm h^{-1} or 25% at 10 mm h^{-1}
  - The random errors between the ground-based and space-based estimates should not exceed 50% at 1 mm h^{-1} or 25% at 10 mm h^{-1}.
- In order to provide data in near-real-time for hurricane monitoring, numerical weather prediction, hydrological model forecast and other application and operational uses:
  - Combined radar/radiometer swath products will be available within 3 hours of observation time, 90% of the time, and
  - Radiometer precipitation products will be available within 1 hour of observation time, 90% of the time.

At the time of the writing of this article all science requirements have been shown to have been met but have not been documented in the literature. Several papers are being prepared on proving these requirements and will be included in the AMS Special Collection of GPM Publications.

Acronym List

AMSR2	Advanced Microwave Scanning Radiometer for Earth Observing System 2
ASCII	American Standard Code for Information Interchange
ATMS	Advanced Technology Microwave Sounder
CNES	Centre National d'Etudes Spatiales
ISRO	Indian Space Research Organisation
CONUS	Continental US
CORRA	Combined Radar-Radiometer Algorithm
dBZ	decibel relative to Z
DMSP	Defense Meteorological Satellite Program
DPR	Dual-frequency Precipitation Radar
EUMESAT	European Union Meteorological Satellites
FOV	Field of View
4D	Four-dimensional
GCOM-W1	Global Change Observation Mission - Water
GCPEx	Global Precipitation Measurement Cold Season Precipitation Experiment
GIS	Geographic Information System
GHz	Gigahertz
GMI	GPM Microwave Imager
GPCP	Global Precipitation Climatology Project
GPM	Global Precipitation Measurement
GPM-CO	Global Precipitation Measurement Core Observatory

GPROF	Goddard Profiling Algorithm
GRACE	Gravity Recovery and Climate Experiment
GSFC	Goddard Space Flight Center
GSMaP	Global Satellite Mapping of Precipitation
GV	Ground Validation
HDF5	Hierarchical Data Format
IMERG	Integrated Multi-satellitE Retrievals for GPM
IR	Infrared
JAXA	Japan Aerospace Exploration Agency
JPSS1	Joint Polar Satellite System-1
JST	Japan Standard Time
LIS	Land Information System
MAE	Mean Absolute Error
MHS	Microwave Humidity Sounder
MHz	Megahertz
MOS	Mission Operations System
MRE	Mean Relative Error
MRMS	Multi-Radar/Multi-Sensor
MSFC	Marshall Space Flight Center
NASA	National Aeronautics and Space Administration
NEDT	Noise Equivalent Delta Temperature
NEXRAD	Next-Generation Radar

NOAA	National Oceanic and Atmospheric Administration
NPP	NASA Postdoctoral Program
NRT	Near-Real-Time
NS	Normal Scan
NWS	National Weather Service
PMM	Precipitation Measurement Missions
PPS	Precipitation Processing System
QPE	Quantitative Precipitation Estimates
SAPHIR	Sounder for Probing Vertical Profiles of Humidity
SMAP	Soil Moisture Active Passive
SPoRT	Short-term Prediction Research and Transition
SSMIS	Special Sensor Microwave Imager/Sounder
TB	Brightness Temperature
TIFF	Tagged Image File Format
TMI	TRMM Microwave Imager
TRMM	Tropical Rainfall Measuring Mission
3D	Three-Dimensional
U.S.	United States
UTC	Coordinated Universal Time
WMO	World Meteorological Organization
WSR-88D	Weather Surveillance Radar 88 Doppler

REFERENCES

Adler, R. F., and Coauthors, 2003: The version-2 global precipitation climatology project (GPCP) monthly precipitation analysis (1979-present). *J. Hydrometeor.*, **4**, 1147-1167.

Adler, R. F., J. J. Wang, , G. Gu, and G. J. Huffman, 2009: A ten-year tropical rainfall climatology based on a composite of TRMM products. *J. of the Meteor. Soc. of Japan*, **87**, 281-293.

Aonashi, K., and Coauthors, 2009: GSMaP Passive Microwave Precipitation Retrieval Algorithm: Algorithm Description and Validation. *J. of the Meteor. Soc. of Japan*, **87A**, 119-136.

Behrangi, A., G. Stephens, R. F. Adler, G. J. Huffman, B. Lambrigtsen, and M. Lebsock, 2014: An Update on the Oceanic Precipitation Rate and Its Zonal Distribution in Light of Advanced Observations from Space. J. Climate, 27, 3957-3965. doi: http://dx.doi.org/10.1175/JCLI-D-13-00679.1

Berg, W., and coauthors, 2016: Intercalibration of the GPM Microwave Radiometer Constellation. J. Atmos. Oceanic Technol. doi:10.1175/JTECH-D-16-0100.1, in press.

Case, J. L., K. D. White, B. Guyer, J. Meyer, J. Srikishen, C. B. Blankenship, and B. T. Zavodsky, 2016: Real-time Land Information System over the Continental U.S. for situational awareness and local numerical weather prediction applications. *30th Conf. Hydrology,* New Orleans, LA, Amer. Meteor. Soc., 3.3. [Available online at https://ams.confex.com/ams/96Annual/webprogram/Paper287812.html]

Carr, N., P. E. Kirstetter, Y. Hong, J. J. Gourley, M. Schwaller, W. Petersen, N.-Y. Wang, R. R. Ferraro, and X. Xue, 2015: The Influence of Surface and Precipitation Characteristics on TRMM Microwave Imager Rainfall Retrieval Uncertainty. *J. Hydrometeor*., **16**, 1596–1614, doi:10.1175/JHM-D-14-0194.1.

Chen, S., and Coauthors, 2013: Evaluation of Spatial Errors of Precipitation Rates and Types from TRMM Space-borne Radar over the southern CONUS. *J. Hydrometeor.*, **14**, 1884–1896.

Curtis, S., A. Salahuddin, R. F. Adler, G. J. Huffman, G. Gu, and Y. Hong, 2007: Precipitation extremes estimated by GPCP and TRMM: ENSO relationships. *J. of Hydrometeor.*, **8**, 678-689.

Draper, D. W., D. A. Newell, D. A. Teusch, and P. K. Yoho, 2013: Global Precipitation Measurement Microwave Imager (GMI) hot load calibration. *IEEE Trans. Geosci. Rem. Sens*., **51**, 4731-4742, doi:10.1109/TGRS.2013.2239300.

Draper, D. W., D. A. Newell, F. J. Wentz, S. Krimchansky, and G. Skofronick-Jackson, 2015a: The Global Precipitation Measurement (GPM) Microwave Imager (GMI): Instrument Overview and Early On-orbit Performance. *IEEE J. Sel. Topics Geosci. Remote Sens*., **8**, 3452-3462, doi:10.1109/JSTARS.2015.2403303.

595 Draper, D. W., D. A. Newell, D. McKague and J. Piepmeier, 2015b: Assessing Calibration
596 Stability using the Global Precipitation Measurement (GPM) Microwave Imager (GMI)
597 Noise Diodes. *IEEE J. Sel. Topics Geosci. Remote Sens*., **8**,
598 doi:10.1109/JSTARS.2015.2406661.
599 Entekhabi, D., and Coauthors, 2010: The soil moisture active passive (SMAP) mission.
600 *Proceedings of the IEEE*, **98**, 704-716.
601 Grecu, M., W. S. Olson, S. J. Munchak, S. Ringerud, L. Liao, Z. S. Haddad, B. L. Kelley, and S.
602 F. McLaughlin, 2016: The GPM Combined Algorithm. *J. Atmos. Oceanic Technol.*, **33**,
603 2225-2245.
604 Hou, A.Y., G. Skofronick-Jackson, C. Kummerow, and J. M. Shepherd, 2008: Global
605 Precipitation Measurement, *Chapter 6 in Precipitation: Advances in Measurement,*
606 *Estimation and Prediction*, S. Michaelides, Ed., Springer-Verlag, 540 pp.
607 Hou, A. Y., 2013: NASA GPM Science Implementation Plan,
608 https://pmm.nasa.gov/sites/default/files/document_files/GPM%20Science%20Implement
609 ation%20Plan%20-%20April%202013.pdf
610 Hou, A. Y., R. K. Kakar, S. A. Neeck, A. Azarbarzin, C. D. Kummerow, M. Kojima, R. Oki, K.
611 Nakamura, and T. Iguchi, 2014: The Global Precipitation Measurement Mission. *Bull.*
612 *Amer. Meteor. Soc*., **95**, 701-722, doi:10.1175/BAMS-D-13-00164.1.
613 Houze, R. A., K. L. Rasmussen, M. D. Zuluaga, and S. R. Brodzik, 2015: The variable nature of
614 convection in the tropics and subtropics: A legacy of 16 years of the Tropical Rainfall
615 Measuring Mission satellite. *Reviews of Geophysics*, **53**, 994-1021.
616 Huffman, G. J., D. T. Bolvin, D. Braithwaite, K. Hsu, R. Joyce, P. Xie, 2015: Algorithm
617 Theoretical Basis Document (ATBD) Version 4.5 for the NASA Global Precipitation
618 Measurement (GPM) Integrated Multi-satellitE Retrievals for GPM (I-MERG). *GPM*
619 *Project*, Greenbelt, MD, 30 pp. [Available online at
620 http://pmm.nasa.gov/sites/default/files/document_files/ IMERG_ATBD_V4.5.pdf]
621 Jedlovec, G., 2013: Transitioning Research Satellite Data to the Operational Weather
622 Community: The SPoRT Paradigm. *Geoscience and Remote Sensing Newsletter*, March,
623 L. Bruzzone, Ed., Institute of Electrical and Electronics Engineers, Inc., New York, 62-
624 66.
625 Kidd, C., A. Becker, G. J. Huffman, C. L. Muller, P. Joe, G. Skofronick-Jackson, D. B.
626 Kirschbaum, 2016: So, How Much of the Earth's Surface Is Covered by Rain Gauges?
627 *Bull. Amer. Meteor. Soc.*, **97**, in early release. doi:10.1175/BAMS-D-14-00283.1.
628 Kirschbaum, D. B., and Coauthors, 2016: NASA's Remotely-sensed Precipitation: A Reservoir
629 for Applications Users, *Bull. Amer. Meteor. Soc*, submitted.
630 Kirschbaum, D. B., and K. Patel, 2016: Precipitation data key to food security and public health.
631 *Eos* https://eos.org/meeting-reports/precipitation-data-key-to-food-security-and-public-
632 health.

Kirstetter, P. E., Y. Hong, J. J. Gourley, Q. Cao, M. Schwaller, and W. Petersen, 2014: A research framework to bridge from the Global Precipitation Measurement mission core satellite to the constellation sensors using ground radar-based National Mosaic QPE. In L. Venkataraman, Remote Sensing of the Terrestrial Water Cycle. AGU books Geophysical Monograph Series, Chapman monograph on remote sensing. John Wiley & Sons Inc. ISBN: 1118872037.

Kirstetter, P. E., Y. Hong, J. J. Gourley, S. Chen, Z. Flamig, J. Zhang, M. Schwaller, W. Petersen, and E. Amitai, 2012: Toward a Framework for Systematic Error Modeling of Spaceborne Precipitation Radar with NOAA/NSSL Ground Radar-based National Mosaic QPE. *J. of Hydrometeor.*, **13**, 1285-1300.

Kirstetter, P. E., Y. Hong, J. J. Gourley, M. Schwaller, W. Petersen, and Q. Cao, 2015a: Impact of sub-pixel rainfall variability on spaceborne precipitation estimation: evaluating the TRMM 2A25 product. *Quart. J. of the Roy. Meteor. Soc.*, **141**, 953–966.

Kirstetter, P.E., J.J. Gourley, Y. Hong, J. Zhang, S. Moazamigoodarzi, C. Langston, A. Arthur, 2015b: Probabilistic Precipitation Rate Estimates with Ground-based Radar Networks. Water Resources Research, 51, 1422–1442. doi:10.1002/2014WR015672

Kojima, M., and Coauthors, 2012: Dual-frequency precipitation radar (DPR) development on the global precipitation measurement (GPM) core observatory. Earth Observing Missions and Sensors: Development, Implementation, and Characterization II, H. Shimoda et al., Eds., International Society for Optical Engineering (SPIE Proceedings, Vol. 8528), 85281A, doi: 10.1117/12.976823.

Kozu, T., and Coauthors, 2001: Development of Precipitation Radar onboard the Tropical Rainfall Measuring Mission satellite. *IEEE Geosci. Remote Sens. Lett.*, **39**, 102–116.

Kubota, T., and Coauthors, 2007: Global Precipitation Map using Satelliteborne Microwave Radiometers by the GSMaP Project: Production and Validation, *IEEE Trans. Geosci. Remote Sens.*, Vol. 45, No. 7, pp.2259-2275.

Kubota, T., and Coauthors, 2014: Evaluation of precipitation estimates by at-launch codes of GPM/DPR algorithms using synthetic data from TRMM/PR observations," IEEE J. Sel. Topics Appl. Earth Observ. Remote Sens., vol.7, no.9, pp. 3931-3944. doi:10.1109/JSTARS.2014.2320960

Kubota, T., T. Iguchi, M. Kojima, L. Liao, T. Masaki, H. Hanado, R. Meneghini, and R. Oki, 2016: A statistical method for reducing sidelobe clutter for the Ku-band precipitation radar onboard the GPM Core Observatory. *J. Atmos. Oceanic Technol.*, 33 (7), 1413-1428.

Kucera, P. A., E. E. Ebert, F. J. Turk, V. Levizzani, D. Kirschbaum, F. J. Tapiador, A. Loew, and M. Borsche, 2013: Precipitation from space: Advancing Earth system science. *Bull. Amer. Meteor. Soc.*, **94**, 365-375.

Kumar, S. V, and Coauthors, 2006: Land Information System - An Interoperable Framework for High Resolution Land Surface Modeling. *Environ. Model. Softw.*, **21**, 1402–1415.

Kummerow, C. D., D. L. Randel, M. Kulie, N.-Yu Wang, R. Ferraro, S. J. Munchak, and V. Petkovic, 2015: The Evolution of the Goddard PROFiling Algorithm to a Fully Parametric Scheme. *J. Atmos. Oceanic Technol.*, **32**, 2265–2280.

Kummerow, C., W. Barnes, T. Kozu, J. Shiue, and J. Simpson, 1998: The Tropical Rainfall Measuring Mission (TRMM) Sensor Package, *J. Atmos. Oceanic Technol.*, **15,** 809–817.

Kummerow, C., and Coauthors, 2000: The status of the Tropical Rainfall Measuring Mission (TRMM) after two years in orbit, *J. Appl. Meteor*., **39**, Part 1, 1965-1982.

Kummerow, C. D., S. Ringerud, J. Crook, D. Randel, and W. Berg, 2010: An observationally generated *A-Priori* database for microwave rainfall retrievals, *J. Atmos. Oceanic Tech*., **28**, 113-130, doi:10.1175/2010JTECHA1468.1.

Le Vine, D. M., G. S. E. Lagerloef, and S. E. Torrusio. 2010: Aquarius and remote sensing of sea surface salinity from space. *Proceedings of the IEEE*, **98**, 688-703.

Liu, N. and C. Liu, 2016: Global distribution of deep convection reaching tropopause in 1 year GPM observations. *J. of Geophys. Res.: Atmos.*, **121**, 3824-3842.

Liu, C., D. J. Cecil, E. J., Zipser, K. Kronfeld, and R. Robertson, 2012: Relationships between lightning flash rates and radar reflectivity vertical structures in thunderstorms over the tropics and subtropics. *J. of Geophys. Res.: Atmos.*, **117,** 19 pp. doi:10.1029/2011JD017123.

Liu, C. and E. J. Zipser, 2015: The global distribution of largest, deepest, and most intense precipitation systems. *Geophy. Res. Lett.*, **42**, 3591-3595.

Prakash, S., Mitra, A. K., D. S. Pai, and A. AghaKouchak, 2016: From TRMM to GPM: How well can heavy rainfall be detected from space?. *Advances in Water Resources*, **88**, 1-7.

Panegrossi, G., and Coauthors, 2015: Use of the constellation of PMW radiometers in the GPM ERA for heavy precipitation event monitoring and analysis during fall 2014 in Italy. In *2015 IEEE International Geoscience and Remote Sensing Symposium (IGARSS)*, 5150-5153).

Peters-Lidard, C. D., and Coauthors, 2007: High-performance Earth system modeling with NASA/GSFC's Land Information System. *Innovations Syst. Softw. Eng.*, **3,** 157-165.

Seto, S., T. Iguchi, T. Shimozuma, and S. Hayashi, 2015: NUBF correction methods for the GPM/DPR level-2 algorithms. In *2015 IEEE International Geoscience and Remote Sensing Symposium (IGARSS)*, 2612-2614.

Shepherd, M., T. Mote, J. Dowd, M. Roden, P. Knox, S. C. McCutcheon, S. E. Nelson, 2011: An overview of synoptic and mesoscale factors contributing to the disastrous Atlanta flood of 2009. *Bull. Amer. Meteor. Soc.*, **92**, 861-870.

Simpson, J. R., R. F. Adler, and G. R. North, 1988: A proposed Tropical Rainfall Measuring Mission (TRMM) satellite, *Bull. Amer. Meteor. Soc.*, **69,** 278–295.

Skofronick-Jackson, and Coauthors, 2015: Global Precipitation Measurement Cold Season Precipitation Experiment (GCPEx): For Measurement Sake Let it Snow. *Bull. Amer. Meteor. Soc.*, **96**, 1719–1741, doi:10.1175/BAMS-D-13-00262.1.

SPoRT website, 2016: [Available online at https://nasasport.wordpress.com/category/land-information-system-lis/ accessed June 28, 2016; or http://weather.msfc.nasa.gov/sport/.

Stephens, G. L., and Coauthors, 2002: The CloudSat mission and the A-Train: A new dimension of space-based observations of clouds and precipitation. *Bull. Amer. Meteor. Soc.*, **83**, 1771-1790.

Tapley, B. D., S. Bettadpur, J. C. Ries, P. F. Thompson, and M. M. Watkins, 2004: GRACE measurements of mass variability in the Earth system. *Science*, **305**, 503-505.

Tan, B.-Z, W. A. Petersen, and A. Tokay, 2016 (a): A Novel Approach to Identify Sources of Errors in IMERG for GPM Ground Validation. *J. Hydromet*., in press.

Tan, B.-Z., W. A. Petersen, P. Kirstetter, and Y. Tian, 2016(b): Performance of IMERG as a Function of Spatiotemporal Scale. *J. Hydromet*, in press

Tao, W.-K., and Coauthors, 2016: TRMM latent heating retrieval: Applications and comparisons with field campaigns and large-scale analyses, in Multi-scale Convection-Coupled Systems in the Tropics. *Meteor. Monogr.,* No. 56, 34 pp.

Toyoshima, K., H. Masunaga, and F.A. Furuzawa, 2015: Early Evaluation of Ku-and Ka-Band Sensitivities for the Global Precipitation Measurement (GPM) Dual-Frequency Precipitation Radar (DPR). *SOLA*, **11**, 14-17, doi:10.2151/sola.2015-004.

Ushio, T. and Coauthors, 2009: A Kalman filter approach to the Global Satellite Mapping of Precipitation (GSMaP) from combined passive microwave and infrared radiometric data. *J. Meteor. Soc. Japan*, 87A, 137-151.

Vargas, M., Z. Jiang, J. Ju, and I. A. Csiszar, 2015: Real-time daily rolling weekly Green Vegetation Fraction (GVF) derived from the Visible Imaging Radiometer Suite (VIIRS) sensor onboard the SNPP satellite. *20th Conf. Satellite Meteorology and Oceanography*, Phoenix, AZ, Amer. Meteor. Soc., P210. [Available online at https://ams.confex.com/ams/95Annual/webprogram/Paper259494.html]

Xia, Y., and Coauthors, 2012: Continental-scale water and energy flux analysis and validation for the North American Land Data Assimilation System project phase 2 (NLDAS-2): 1. Intercomparison and application of model products. *J. Geophys. Res.*, **117,** 27 pp. doi:10.1029/2011JD016048.

Ward, A., D. Kirschbaum, and M. Hobish, 2015: Measuring Rain and Snow for Science and Society: The Second GPM Applications Workshop. *Earth Obs.*, **27**, 4–11. http://eospso.nasa.gov/sites/default/files/eo_pdfs/Sep_Oct_2015_color_508.pdf#page=4.

Wentz, F. J. and D. Draper, 2016: On-Orbit Absolute Calibration of the Global Precipitation Measurement Microwave Imager. *J. Atmos. Oceanic Technol.*, **33**, in early release. doi:10.1175/JTECH-D-15-0212.1.

Wentz, F. J., T. Meissner, 2016: Atmospheric Absorption Model for Dry Air and Water Vapor at Microwave Frequencies below 100 GHz Derived from Spaceborne Radiometer Observations. *Radio Science*, **51**, 381-391. doi:10.1002/2015RS005858.

Wilheit, T., 2013: Comparing calibrations of similar conically-scanning window-channel microwave radiometers. *IEEE Trans. Geosci. Rem. Sens*., **51**, 1453-1464. doi:10.1109/TGRS.2012.2207122.

Wilheit, T., W. Berg, H. Ebrahami, R. Kroodsma, D. McKague, V. Payne, and J. Wang, 2015: Intercalibrating the GPM constellation using the GPM microwave imager (GMI). *Geoscience and Remote Sensing Symposium (IGARSS), 2015 IEEE International*, doi:10.1109/IGARSS.2015.7326996.

Zavodsky, B. T., J. L. Case, C. B. Blankenship, W. L. Crosson, and K. D. White, 2013: Application of next-generation satellite data to a high-resolution, real-time land surface model. *Earthzine*, J. Kart, Ed., Institute of Electrical and Electronics Engineers [Available online at http://www.earthzine.org/2013/04/10/application-of-next-generation-satellite-data-to-a-high-resolution-real-time-land-surface-model/.]

Zhang J., and Coauthors, 2011: National Mosaic and multi-sensor QPE (NMQ) system: Description, results, and future plans. *Bull. Amer. Meteor. Soc.,* **92,** 1321-1338.

Zhang, J., and Coauthors, 2016: Multi-Radar Multi-Sensor (MRMS) Quantitative Precipitation Estimation: Initial Operating Capabilities. *Bull. Amer. Meteor. Soc.*, **97**, 621-638.

Table 1: Channel availability by frequency and polarization (V=Vertically polarized, H=Horizontally polarized) for the GPM constellation radiometers. GMI, TMI, AMSR2, and SSMIS are all conically scanning imagers while MHS, ATMS, and SAPHIR are cross-track scanning water vapor sounders. ATMS is currently operating on board Suomi NPP with a second copy to launch on board JPSS1 in mid 2017.

Sensor	Satellite	6-7 GHz	10 GHz	18-19 GHz	21-23 GHz	31-37 GHz	85-92 GHz	150-166 GHz	183 GHz
GMI	GPM		10.65 VH	18.7 VH	23.8 V	36.64 VH	89.0 VH	166 VH	183.31 V ±3, ±7
TMI	TRMM		10.65 VH	19.35 VH	21.3 V	37.0 VH	85.5 VH		
AMSR2	GCOM-W1	6.925 VH 7.3 VH	10.65 VH	18.7 VH	23.8 VH	36.5 VH	89.0 VH		
SSMIS	DMSP F16, F17, F18, F19			19.35 VH	22.235 V	37.0 VH	91.655 VH	150 H	183.31 H ±1, ±3, ±6.6
MHS	NOAA-18/19, MetOp-A/B						89 V	157 V	183.31 H ±1, ±3, 190.31V
ATMS	Suomi NPP, JPSS1				23.8 V	31.4 V	88.2 V	165.5 H	183.31 H ±1, ±1.8, ±3, ±4.5, ±7
SAPHIR	Megha-Tropiques								183.31 H ±0.2, ±1.1, ±2.8, ±4.2, ±6.8, ±11

775 Table 2: Area weighted mean annual precipitation in mm day^{-1} for each of the algorithms

776 globally, over land, and over ocean from +/- 50 degrees latitude.

	Global Mean Daily Precipitation	Oceanic Mean Daily Precipitation	Land Mean Daily Precipitation
DPR	2.51	2.77	1.72
GPROF	2.86	2.99	2.36
Ku	2.81	3.03	2.05
CORRA	2.83	2.85	2.77
IMERG	2.48	2.44	2.39
GPCP	2.95	3.15	2.43
GSMaP	2.74	2.83	2.12

777
778

779 Figure 1: GPM-CO GMI composite brightness temperatures and example precipitation event
780 cases. Center panel: composite 89 GHz brightness temperatures averaged over 24 months
781 showing the latitudinal extent of the GPM-CO measurements. Example precipitation cases (a) A
782 North Pacific frontal system from GMI, (b) Severe storms in Texas from GMI, (c) winter storm
783 over the Eastern U.S. as observed in 3D from the DPR, (d) North Atlantic winter storm from
784 GMI, (e) Typhoon Fantala as observed in 3D from the DPR, (f) Typhoons Chan-Hom and
785 Nangka in two successive orbits from GMI, (g) a South Pacific frontal system from GMI, (h) a
786 South Atlantic frontal system from GMI, (i) a line of convection in Africa in 3D from the DPR,
787 (j-k) Sumatra land/sea convection day and night from GMI, and (l) an Australian weather system
788 from GMI.

789 Figure 2: Integrated Multi-satellitE Retrievals for GPM (IMERG) accumulated precipitation
790 totals from 4-11 August 2014. The IMERG retrieval algorithm has not yet been developed for
791 pole-to-pole retrievals. The large accumulation near Japan is Typhoon Halong. The accumulation
792 also shows a major storm over the North Sea near Europe, the origins of Hurricane Gonzalo on
793 the western coast of Africa, and a deep tropical depression that produced floods across northern
794 India. IMERG gridded products are produced every 30 minutes with 0.1^{o} x 0.1^{o} grid boxes,
795 currently covering the latitude band 60°N-S.

796 Figure 3: Precipitation estimates are shown for a single orbit of each of the GPM constellation
797 radiometer types for January 1, 2015. The conically-scanning window-channel radiometers are
798 shown on the left and the cross-track scanning water vapor sounding radiometers are shown on
799 the right. The constellation radiometers include a) TMI and GMI on board the NASA TRMM
800 and GPM satellites, b) ATMS on board NOAA's Suomi NPP satellite, c) AMSR2 on board

JAXA's GCOM-W1 satellite, d) SAPHIR on board the CNES-ISRO Megha-Tropiques satellite, e) SSMIS on board the DMSP F16, F17, F18 and F19 satellites, and f) MHS on board the NOAA-18, NOAA-19, and EUMETSAT MetOp-A and Metop-B satellites.

Figure 4: GPM mission operations data and communication system. GPM-CO satellite data are downlinked in near-real-time via the NASA Tracking and Data Relay Satellite System (TDRSS) to White Sands, New Mexico, where the GPM Mission Operations Center retrieves it, ensures its integrity and passes it to PPS. Partner data, ancillary information and validation measurements are also processed by mission operations.

Figure 5: Zonal precipitation averages (in mm day^{-1}) for the full annual cycle in 2015. The five estimates are: GPM DPR (dual-frequency radar in red), GPM GPROF (GMI passive radiometer in blue), GPM Ku (single-frequency radar in green), GPM CORRA (DPR+GMI in orange), IMERG (GPM merged with constellation estimates in purple), GPCP global estimates (in light blue), and MCTA2 estimates over ocean (in black, covering the years 2007-2010). The GPCP is Version 2.3, MCTA is Version 2, IMERG is Version 03, and the other GPM products are Version 04.

Figure 6: Density scatterplot of DPR-Normal Scan V04 versus reference MRMS precipitation (mm h^{-1}) at the footprint scale over the period June 2014 - August 2015. The 1:1 line (solid line) is displayed as well as the detection limit for the DPR (0.22 mm h^{-1}). The data shown focuses on

822 the conditional case of satellite footprint and reference mean precipitation rates both nonzero (>
823 0.01 mm h^{-1}), and a precipitation type of liquid only.
824
825 Figure 7: Conditional DPR V04 bias (MRE; solid black line) and random error (mean absolute
826 error; dashed black line) versus the MRMS reference precipitation rate (mm h^{-1}) at 50 km
827 resolution over the period June 2014 - August 2015 and normalized by the bin mean rain rate.
828 Points falling outside of the 5%-95% inter-quantile range (outliers) were not included in this
829 comparison. The dashed red lines indicate the GPM Mission Science Requirements 50% (25%)
830 at the specified precipitation rates of 1.0 (10.0) mm h^{-1}.
831
832 Figure 8: The (a) average and (b) maximum liquid equivalent snowfall rates, and (c) fraction of
833 precipitation that was identified as falling snow (and not liquid rain) from December 2014 –
834 February 2015 from the GMI GPROF (Version 04) retrieval algorithm.
835
836 Figure 9: GPM depicts characteristics of India's monsoon seasons in 2014 and 2015. The time-
837 latitude figure (main panel) summarizes the IMERG precipitation estimates over India from
838 April 2014 through May 2016. The heavy, black, dashed line shows the climatological advance
839 and retreat of India's monsoon. The dates of the climatological advance and retreat are shown
840 also on the two maps on the upper left. The area over which IMERG was averaged is indicated
841 by the blue-gray rectangle stretching across India and the Bay of Bengal; the latitude on the main
842 panel is along the mid-line of the rectangle, and the averages are taken along the perpendiculars
843 to the mid-line.

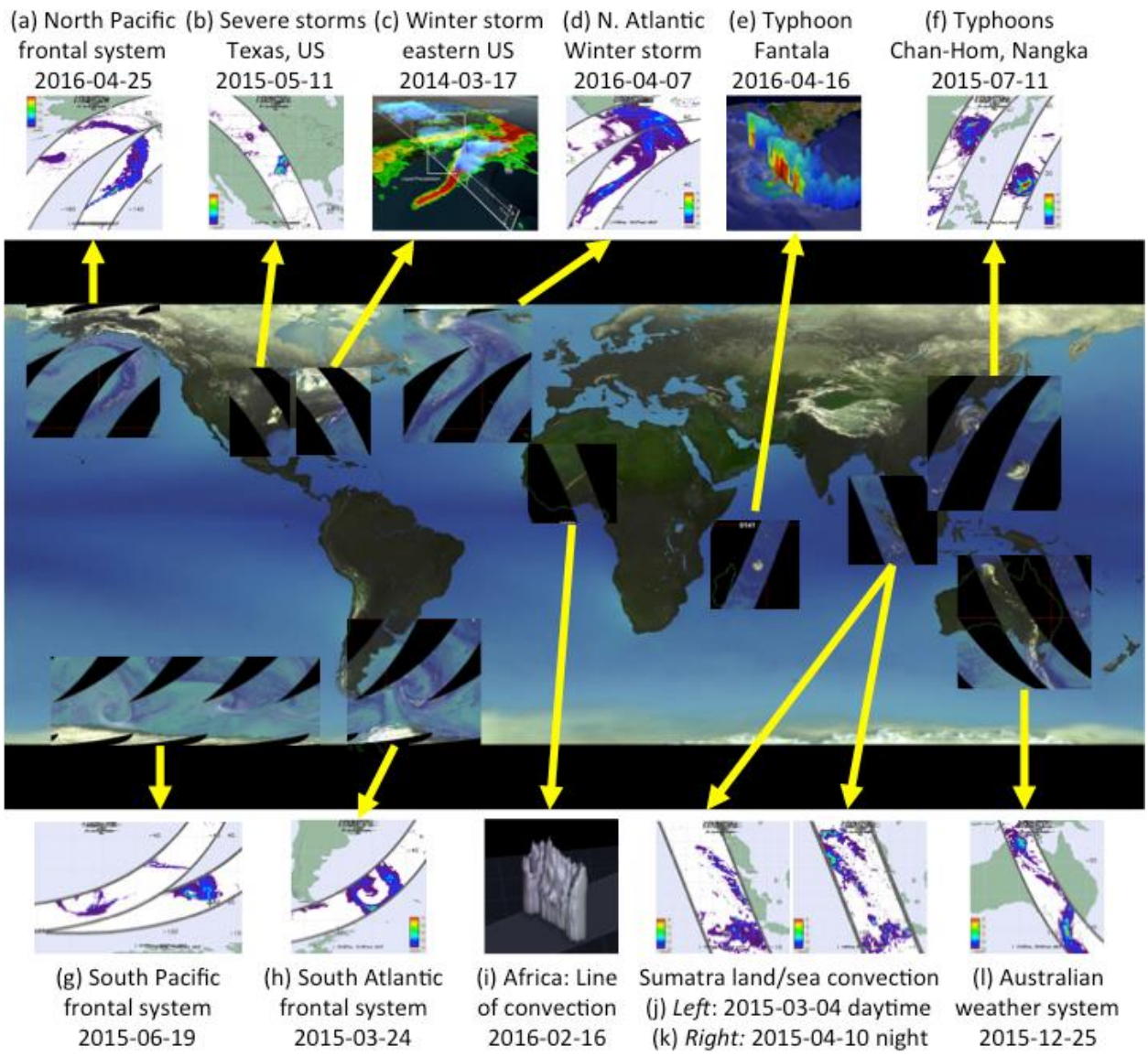

Figure 1: GPM-CO GMI composite brightness temperatures and example precipitation event cases. Center panel: composite 89 GHz brightness temperatures averaged over 24 months showing the latitudinal extent of the GPM-CO measurements. Example precipitation cases (a) A North Pacific frontal system from GMI, (b) Severe storms in Texas from GMI, (c) winter storm over the Eastern U.S. as observed in 3D from the DPR, (d) North Atlantic winter storm from GMI, (e) Typhoon Fantala as observed in 3D from the DPR, (f) Typhoons Chan-Hom and Nangka in two successive orbits from GMI, (g) a South Pacific frontal system from GMI, (h) a South Atlantic frontal system from GMI, (i) a line of convection in Africa in 3D from the DPR, (j-k) Sumatra land/sea convection day and night from GMI, and (l) an Australian weather system from GMI.

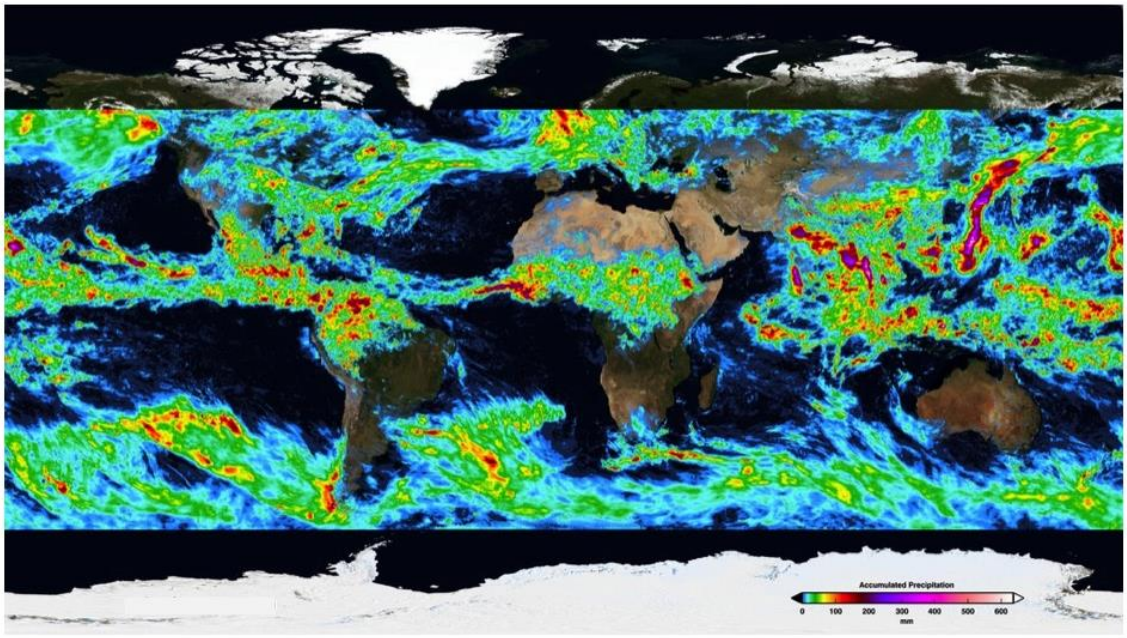

Figure 2: Integrated Multi-satellitE Retrievals for GPM (IMERG) accumulated precipitation totals from 4-11 August 2014. The IMERG retrieval algorithm has not yet been developed for pole-to-pole retrievals. The large accumulation near Japan is Typhoon Halong. The accumulation also shows major storm over the North Sea near Europe, the origins of Hurricane Gonzalo on the western coast of Africa, and a deep tropical depression that produced floods across northern India. IMERG gridded products are produced every 30 minutes with 0.1^{o} x 0.1^{o} grid boxes, currently covering the latitude band 60°N-S.

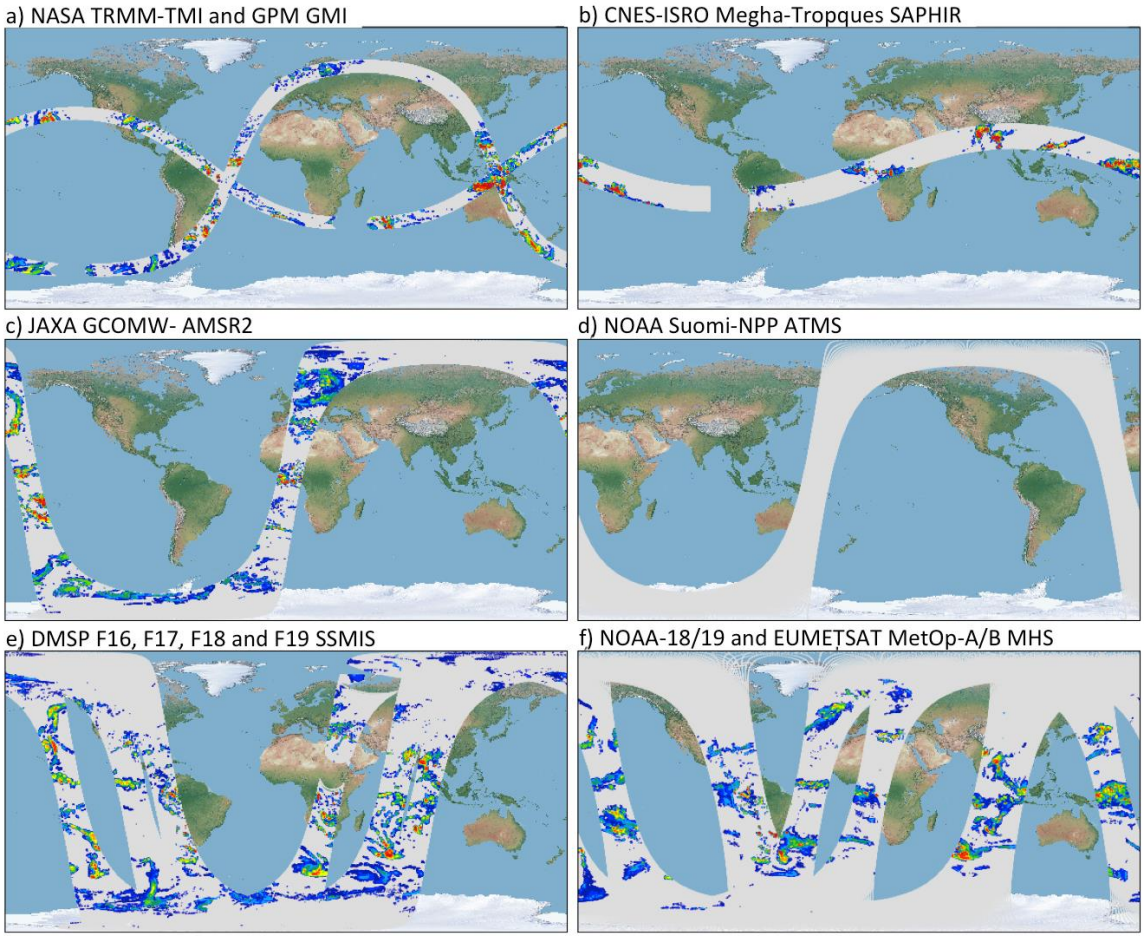

Figure 3: Precipitation estimates are shown for a single orbit of each of the GPM constellation radiometer types for January 1, 2015. The conically-scanning window-channel radiometers are shown on the left and the cross-track scanning water vapor sounding radiometers are shown on the right. The constellation radiometers include a) TMI and GMI on board the NASA TRMM and GPM satellites, b) ATMS on board NOAA's Suomi NPP satellite, c) AMSR2 on board JAXA's GCOM-W1 satellite, d) SAPHIR on board the CNES-ISRO Megha-Tropiques satellite, e) SSMIS on board the DMSP F16, F17, F18 and F19 satellites, and f) MHS on board the NOAA-18, NOAA-19, and EUMETSAT MetOp-A and Metop-B satellites.

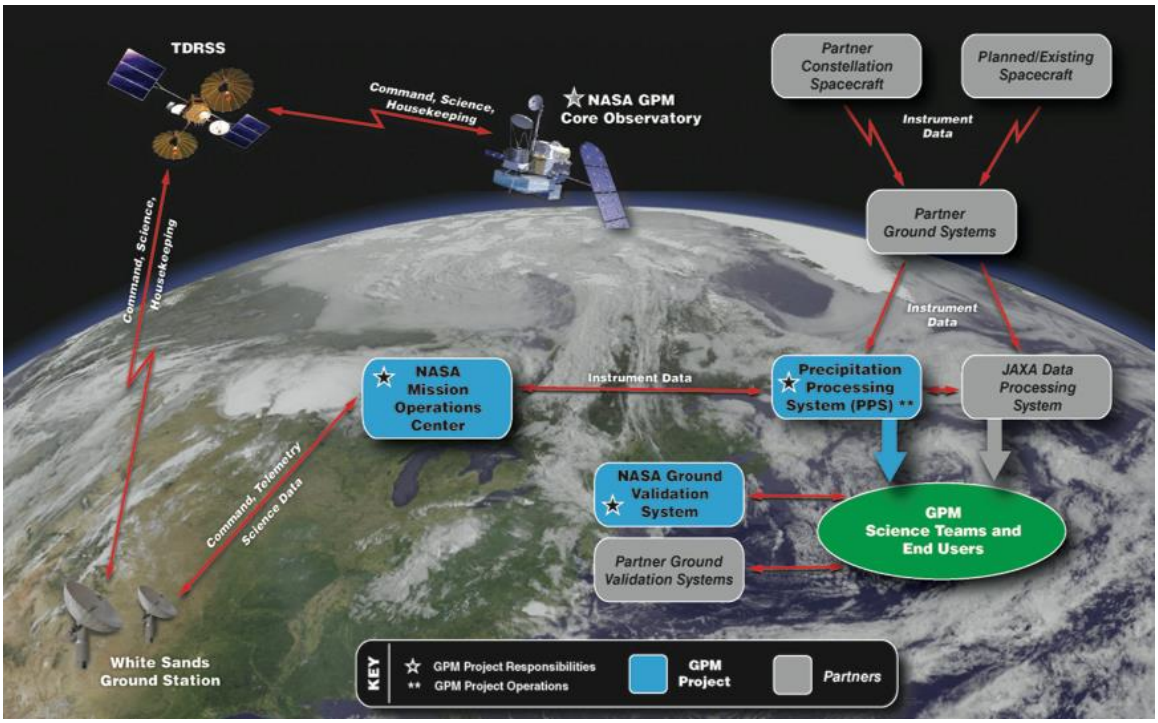

Figure 4: GPM mission operations data and communication system. GPM-CO satellite data are downlinked in near-real-time via the NASA Tracking and Data Relay Satellite System (TDRSS) to White Sands, New Mexico, where the GPM Mission Operations Center retrieves it, ensures its integrity and passes it to PPS. Partner data, ancillary information and validation measurements are also processed by mission operations.

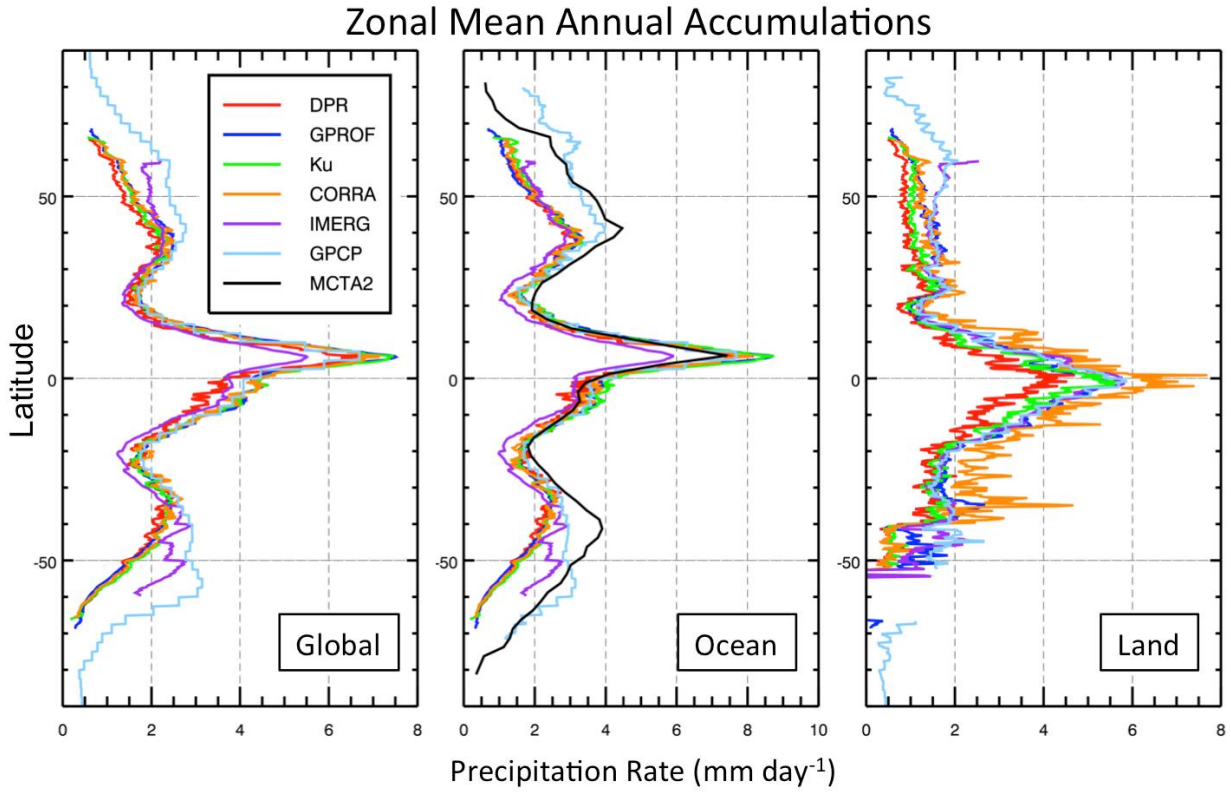

Figure 5: Zonal precipitation averages (in mm day^{-1}) for the full annual cycle in 2015. The five estimates are: GPM DPR (dual-frequency radar in red), GPM GPROF (GMI passive radiometer in blue), GPM Ku (single-frequency radar in green), GPM CORRA (DPR+GMI in orange), IMERG (GPM merged with constellation estimates in purple), GPCP global estimates (in light blue), and MCTA2 estimates over ocean (in black, covering the years 2007-2010). The GPCP is Version 2.3, MCTA is Version 2, IMERG is Version 03, and the other GPM products are Version 04.

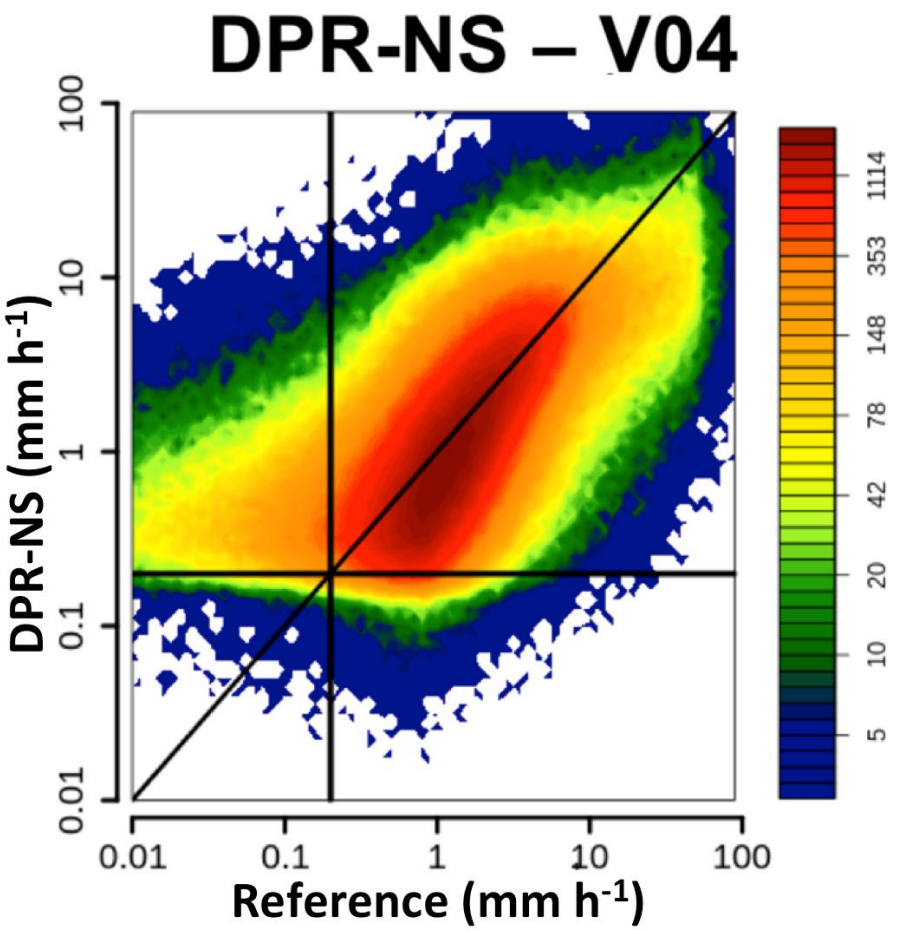

Figure 6: Density scatterplot of DPR-Normal Scan V04 versus reference MRMS precipitation (mm h^{-1}) at the footprint scale over the period June 2014 - August 2015. The 1:1 line (solid line) is displayed as well as the detection limit for the DPR (0.22 mm h^{-1}). The data shown focuses on the conditional case of satellite footprint and reference mean precipitation rates both nonzero (> 0.01 mm h^{-1}), and a precipitation type of liquid only.

907

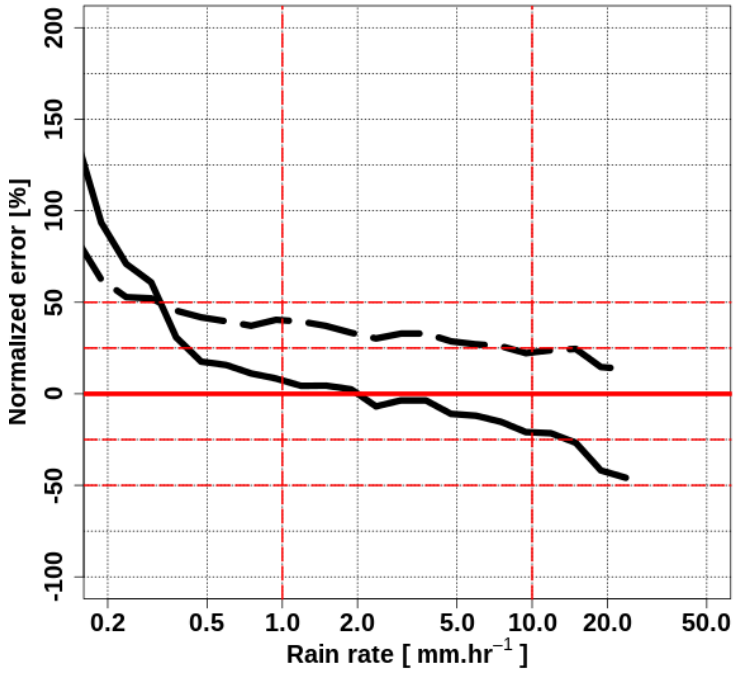

908

909 Figure 7: Conditional DPR V04 bias (MRE; solid black line) and random error (mean absolute
910 error; dashed black line) versus the MRMS reference precipitation rate (mm h^{-1}) at 50 km
911 resolution over the period June 2014 - August 2015 and normalized by the bin mean rain rate.
912 Points falling outside of the 5%-95% inter-quantile range (outliers) were not included in this
913 comparison. The dashed red lines indicate the GPM Mission Science Requirements 50% (25%)
914 at the specified precipitation rates of 1.0 (10.0) mm h^{-1}.

915

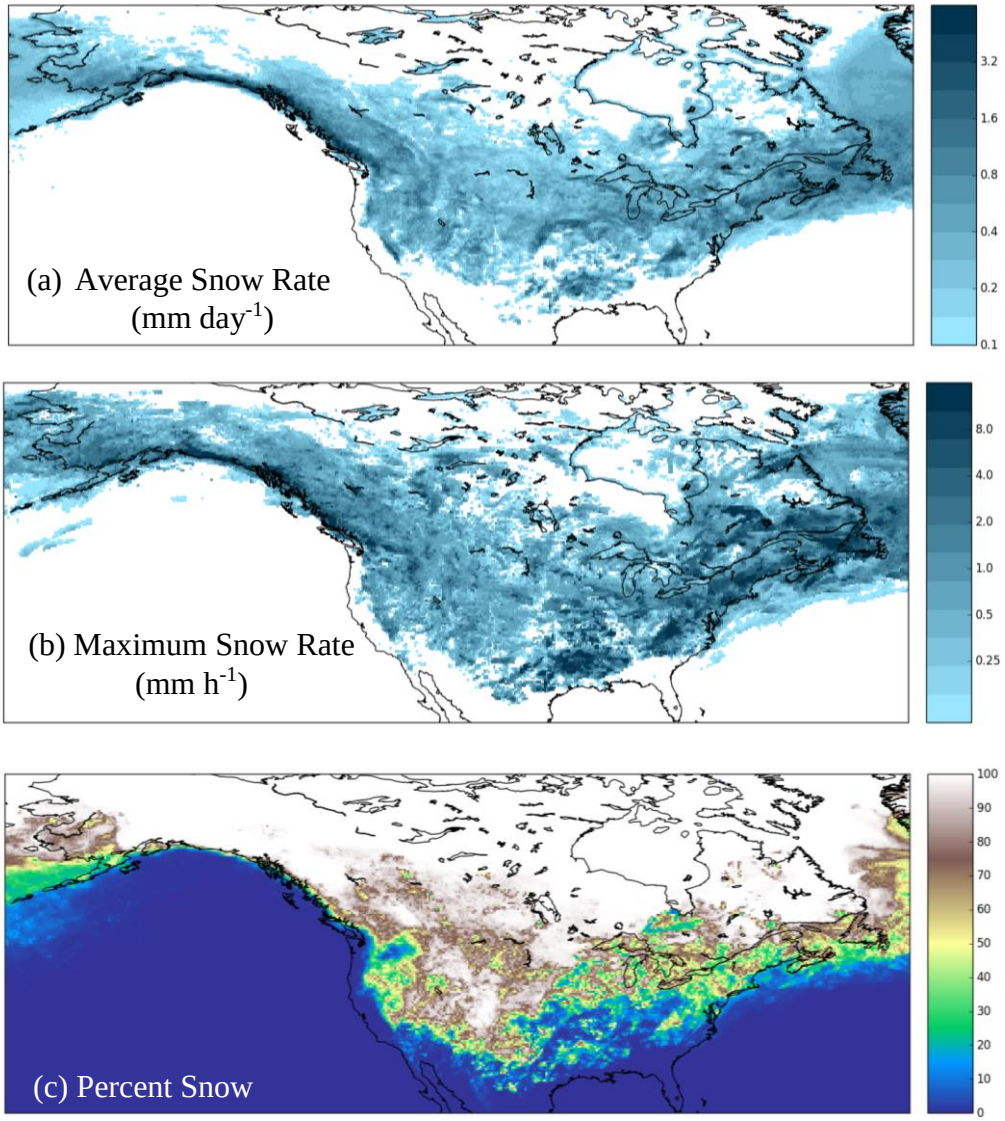

Figure 8: The (a) average and (b) maximum liquid equivalent snowfall rates, and (c) fraction of precipitation that was identified as falling snow (and not liquid rain) from December 2014 – February 2015 from the GMI GPROF (Version 04) retrieval algorithm. The average snow rate includes zeros. The maximum is the maximum observed over the whole time period.

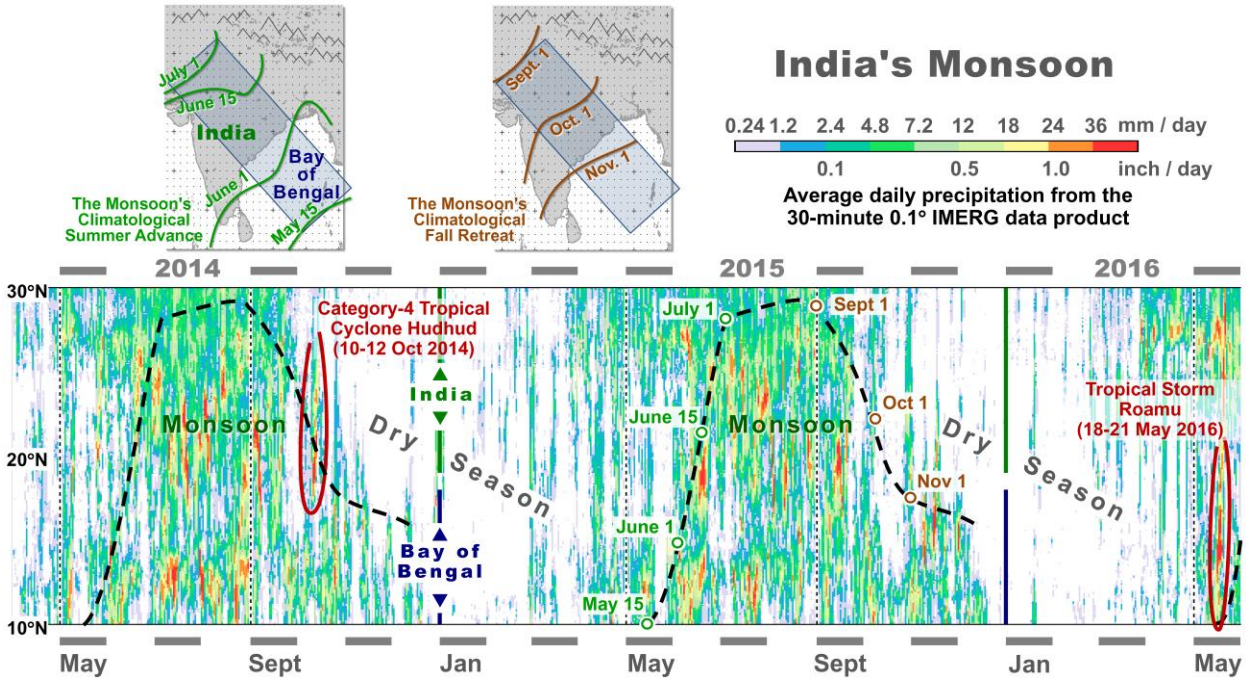

Figure 9: GPM depicts characteristics of India's monsoon seasons in 2014 and 2015. The time-latitude figure (main panel) summarizes the IMERG precipitation estimates over India from April 2014 through May 2016. The heavy, black, dashed line shows the climatological advance and retreat of India's monsoon. The dates of the climatological advance and retreat are shown also on the two maps on the upper left. The area over which IMERG was averaged is indicated by the blue-gray rectangle stretching across India and the Bay of Bengal; the latitude on the main panel is along the mid-line of the rectangle, and the averages are taken along the perpendiculars to the mid-line.